

Cite this: Phys. Chem. Chem. Phys., 2011, 13, 5388–5393

www.rsc.org/pccp PAPER

Microscopic structure and dynamics of air/water interface by computer simulations—comparison with sum-frequency generation experiments†

Yanting Wang, A Nathan O. Hodas, *bc Yousung Jungd and R. A. Marcusb

Received 2nd December 2010, Accepted 9th February 2011 DOI: 10.1039/c0cp02745f

The air/water interface was simulated and the mode amplitudes and their ratios of the effective nonlinear sum-frequency generation (SFG) susceptibilities ($A_{\rm eff}$'s) were calculated for the ssp, ppp, and sps polarization combinations and compared with experiments. By designating "surface-sensitive" free OH bonds on the water surface, many aspects of the SFG measurements were calculated and compared with those inferred from experiment. We calculate an average tilt angle close to the SFG observed value of 35, an average surface density of free OH bonds close to the experimental value of about 2.8×10^{18} m⁻², computed ratios of $A_{\rm eff}$'s that are very similar to those from the SFG experiment, and their absolute values that are in reasonable agreement with experiment. A one-parameter model was used to calculate these properties. The method utilizes results available from independent IR and Raman experiments to obtain some of the needed quantities, rather than calculating them ab initio. The present results provide microscopic information on water structure useful to applications such as in our recent theory of on-water heterogeneous catalysis.

Introduction

The hydrogen (H) bonded structure of water at the air/water interface 1-5 is of fundamental interest because it determines the properties of aqueous interfaces and their reactivity. Certain atmospheric reactions, 6 such as those involved in ozone depletion, are known to be catalyzed by the ice surface on cloud particles. Study of the air/water interface is also important for understanding more complicated organic/water interfaces 5 that have recently begun to attract interest for its potential for rate acceleration 7 of organic reactions and green chemistry in emulsions. For example, interest in catalytic effects of dangling OH's has also been extended to their role in catalysis of different organic reactions by metal oxides enriched in surface OH groups. 8

The first molecular structure of water at the air/water interface using the surface-specific vibrational sum-frequency generation (SFG) technique was reported by Du *et al.*⁹ in 1993.^{1,10} In that

work, using the "titration" of dangling OH groups with methanol and hence the complete suppression of the peak of the free OH SFG signal, it was found that about 25% of surface water molecules have one dangling OH bond that is not H-bonded to other water molecules. It is thereby free, and protrudes out of the water phase, confirming earlier predictions from computations.¹¹ Roughly the same picture of the existence of the free OH bonds at the interface has since been consistently observed in SFG experiments by Richmond,⁵ Eisenthal, ¹² Allen, ¹³ and Gan *et al.*, ¹⁴ and also in computer simulations. ^{3,15–19} The structure of water at the hydrophobic organic/water interfaces was shown to be similar to that at the air/water interface. 9,20,21 In the process of understanding the air/water interface, different interpretations were also made in terms of details of the air/water interface using both experiments and computations. 1,22-24 Although previous work has made significant progress toward explaining the observed SFG spectra using theory and simulation, 5,16,25-27 a complete picture of how rapid motion averages out the SFG has not been presented. In the present article, we make a quantitative comparison between multiple experimental observables, going beyond the comparison of ratios. In addition, by utilizing independent experimental results, coupled with molecular dynamics simulation of the air/water interface, the present work has as a goal a better understanding of motional averaging in SFG. This study was prompted by the recent "on-water" catalysis experiments and our interpretation in terms of the role of dangling OH groups at the water-oil emulsion interface.²⁸

The orientation of free OH bonds at the air/water interface has been deduced from several SFG experiments to be nearly

^a Key Laboratory of Frontiers in Theoretical Physics, Institute of Theoretical Physics and Kavli Institute for Theoretical Physics China, Chinese Academy of Sciences, 55 Zhongguancun East Road, Beijing 100190, P. R. China

b Department of Chemistry, California Institute of Technology, Pasadena, CA 91125. E-mail: hodas@caltech.edu

^c Department of Physics, California Institute of Technology, Pasadena, CA 91125

d Graduate School of Energy, Environment, Water, and Sustainability (WCU), Korea Advanced Institute of Science and Technology (KAIST), Daejeon 305-701, Korea

[†] This article is part of the special collection on *Interfacial processes* and mechanisms in celebration of John Albery's 75th birthday.

perpendicular to the surface plane. 9,14,29 An SFG interpretation 29 assumed a step-like distribution for the tilt angles (θ_{OH}) between the free OH bonds and the surface normal, suggesting them to be in the interval $0^{\circ} \le \theta_{OH} \le 51^{\circ}$, yielding an average tilt angle $\langle \theta_{\rm OH} \rangle \approx 35^{\circ}$. A more recent SFG experiment¹⁴ yielded a similar average tilt angle, $\langle \theta_{OH} \rangle \approx 30^{\circ}$, with a narrow distribution width of $\leq 15^{\circ}$, assuming a Gaussian distribution model. In contrast to these distributions and average orientations of free OH bonds, however, previous molecular dynamics simulations^{3,15–18,30} with various water models consistently predicted widths of the orientational distribution much broader than those assumed in the previous interpretations of SFG experiments.^{1,9,14,29} We address this discrepancy by considering the nature of free OH bonds on the surface, and, in a procedure detailed below, selectively removing those that would likely not contribute to the SFG, allowing a direct comparison between our calculations and experimental measurements.

Methods

The theoretical treatment we use in this paper to calculate the effective SFG nonlinear susceptibilities originated from the one previously developed in the literature^{9,29} to extract the orientation information of interfacial molecules from SFG experiments. Previous reviews have provided details of the treatment. 31,32 Here, we summarize the assumptions and key expressions, for completeness, and implement the expressions to obtain the forms that are suitable for numerical calculations of the mode amplitudes by explicit integrals, rather than the more simplified fast and slow approximations.²⁹

The SFG signal is proportional to the square of the effective nonlinear susceptibility, $\chi_{\text{eff}}^{(2)}(\omega)$, which is a sum of resonant, $\chi_{R,\text{eff}}^{(2)}(\omega)$, and nonresonant, $\chi_{NR,\text{eff}}^{(2)}(\omega)$, contributions: 1,10

$$\chi^{(2)}_{\rm eff}(\omega) = \chi^{(2)}_{\rm NR,eff} + \chi^{(2)}_{R,\rm eff} = \chi^{(2)}_{\rm NR,eff} + \sum_q \frac{A_{q,\rm eff}}{\omega - \omega_q + i \Gamma_q} \ \ (1)$$

where ω is the incident infrared frequency, ω_q is the qth vibrational frequency, $A_{q,\text{eff}}$ is the mode amplitude, and Γ_q is the damping constant for the qth molecular vibrational mode. The sum-frequency spectra are obtained by scanning the IR frequencies that probe the vibrational normal modes, using the IR-visible SFG method. The susceptibility originates at the air/water interface, caused by the symmetry breaking at the boundary. The bulk of the fluid has inversion symmetry and so does not contribute to techniques generating second-order nonlinear polarization.

SFG is approximated to be dipolar in origin, and we neglect any quadrupolar contribution that could emanate from the bulk. In this paper we focus on the free OH stretching mode of water molecules at the air/water interface, $\omega_a = 3698 \text{ cm}^{-1}$. This stretching frequency corresponds to the water configuration where one OH bond is free while the other OH bond of the same parent water molecule is still H-bonded to neighboring water molecules (so-called "single-donor" configuration). The spectra for the ssp, ppp, and sps combinations of polarization, labeled in the order of the sum frequency output,

visible input, and infrared input fields, are obtained in SFG experiments.

The A_{eff} 's in eqn (1) can be related to the intrinsic tensor components via the Fresnel factors, i.e. via the macroscopic local field corrections, L_{ii} , 31

$$A_{\text{eff}}(ssp) = L_{yy}(\omega_s)L_{yy}(\omega_1)L_{zz}(\omega_2)\sin \beta_2 A_{yyz}$$

$$A_{\text{eff}}(ppp) = -L_{xx}(\omega_s)L_{xx}(\omega_1)L_{zz}(\omega_2)\cos\beta_s\cos\beta_1\sin\beta_2A_{yyz}$$

$$-L_{xx}(\omega_s)L_{zz}(\omega_1)L_{xx}(\omega_2)\cos\beta_s\sin\beta_1\cos\beta_2A_{yzy}$$

$$+L_{zz}(\omega_s)L_{xx}(\omega_1)L_{xx}(\omega_2)\sin\beta_s\cos\beta_1\cos\beta_2A_{zyy}$$

$$+L_{zz}(\omega_s)L_{zz}(\omega_1)L_{zz}(\omega_2)\sin\beta_s\sin\beta_1\sin\beta_2A_{zzz}$$

$$A_{\text{eff}}(sps) = L_{yy}(\omega_s)L_{zz}(\omega_1)L_{yy}(\omega_2)\sin\beta_1 A_{yzy}$$
 (2)

where β_S , β_1 , and β_2 are the reflected or incident angles of sum frequency output, visible input, and infrared input, respectively. For an azimuthally isotropic air/water interface and assuming the visible frequency (ω_1) and the sum frequency (ω_S) are far removed from the electronic resonances, there are only three independent nonvanishing components, $A_{xxz} = A_{yyz}$, $A_{xzx} = A_{yzy} = A_{zxx} = A_{zyy}$, and A_{zzz} . The ω_2 is the infrared input light source and the L_{ii} 's are defined in terms of the frequency-dependent effective dielectric constant of the interfacial layer, $\varepsilon(\omega)$, an air/water interface in our case. For the air/water interface, $\varepsilon(\omega_S) = \varepsilon(\omega_1) = 1.31$ and $\varepsilon(\omega_2) = 1.2$ were estimated²⁹ from a 3-layer model. The numerical values of all these variables can be found in Table 1 of ref. 29. The A_{iik} 's are intrinsic (macroscopic) properties of the interface, whereas the experimental observables, A_{eff} 's, are affected by the frequencydependent dielectric response of the interface medium as described above and by the experimental conditions. Therefore, using eqn (2), we use the above ε 's to obtain A_{eff} 's from the calculated A_{ijk} 's.

The A_{ijk} 's in eqn (2) are the resonant components of macroscopic susceptibility tensor, and can be represented at a molecular level as an ensemble average of the molecular hyperpolarizability in the body fixed frame, $\beta_{q,\lambda\mu\nu}$ (corresponding to the hyperpolarizability A_q of Du et al.⁹), of the interfacial water molecules in the lab frame (denoted by ijk), where q corresponds to the IR resonant mode of the free OH bond. The derivation begins with the Fourier-Laplace transform of the classical SFG response function: related references are 26,29,33-36

$$A_{ijk} \equiv (\omega_2 - \omega_q + i\Gamma_q)\chi_{R,ijk}^{(2)}$$

$$= -(\omega_2 - \omega_q + i\Gamma_q)(k_BT)^{-1}$$

$$\times \int_0^\infty e^{i\omega_2 t} \langle \alpha_{ij}(0)\mu_k(t)\rangle dt, \tag{3}$$

Table 1 Average number of free OH, $\langle n_{\text{OH}} \rangle$, and average orientation angle, $\langle \theta_{\rm OH} \rangle$, of free surface OH bonds calculated from three MD simulations with different snapshot time intervals

Snapshot interval	$\langle n_{ m OH} angle$	$\langle heta_{ m OH} angle$	
1 fs	26	38°	
10 fs	26	38°	
100 fs	26	38°	

where α_{ij} is the instantaneous polarizability tensor of the entire surface, and μ_k is the instantaneous dipole moment vector of the surface. Eqn (3) can be expanded as

$$A_{ijk} = -(\omega_2 - \omega_q + i\Gamma_q) \sum_{\lambda\mu\nu} (k_{\rm B}T)^{-1} \alpha_{\lambda\mu} \mu_{\nu}$$

$$\times \int_0^\infty dt e^{i\omega_2 t} \left\langle \sum_n^{N_{\rm OH}(0)} \sum_m^{N_{\rm OH}(t)} D_{i\lambda}^n(0) D_{j\mu}^n(0) D_{k\nu}^m(t) \right\rangle$$
(4)

where the sum of λ , μ , or ν is over \hat{u} , \hat{v} , or \hat{w} , the basis of the body-fixed molecular reference frame. Similarly, $i=\hat{x}$, \hat{y} , \hat{z} , the laboratory frame basis, and the same for j and k. The sum includes the nth and mth free surface OH bonds at times 0 and t, respectively. At time t there are $N_{\rm OH}(t)$ free OH bonds. $D^n_{i\lambda}$, $D^n_{j\mu}$, and $D^m_{k\nu}$ are the time-dependent direction cosine matrix elements for the nth and mth free surface OH bonds, defined as $D_{xu}=\hat{x}\cdot\hat{u}$. Eqn (4) is a generalization of equations in Wei and Shen, and it can be shown to reduce to corresponding approximations of slow and fast orientational dynamics. Given this, however, eqn (4) also explicitly incorporates spatial correlations between water molecules, unlike those in Wei and Shen, which use a mean-field approximation.

Comparison with the experimental results of Wei and Shen requires calculating the absolute value of the A_{eff} 's. After substituting in the hyperpolarizability, we then calculate the quantities:

$$\operatorname{Re} A_{ijk} = -\Gamma_{q} \sum_{\lambda\mu\nu} \beta_{q,\lambda\mu\nu} \int_{0}^{\infty} dt \cos(\omega_{q} t)$$

$$\times \left\langle \sum_{n}^{N_{\mathrm{OH}}(0)} \sum_{m}^{N_{\mathrm{OH}}(t)} D_{i\lambda}^{n}(0) D_{j\mu}^{n}(0) D_{k\nu}^{m}(t) \right\rangle,$$

$$\operatorname{Im} A_{ijk} = -\Gamma_{q} \sum_{\lambda\mu\nu} \beta_{q,\lambda\mu\nu} \int_{0}^{\infty} dt \sin(\omega_{q} t)$$

$$\times \left\langle \sum_{n}^{N_{\mathrm{OH}}(0)} \sum_{m}^{N_{\mathrm{OH}}(t)} D_{i\lambda}^{n}(0) D_{j\mu}^{n}(0) D_{k\nu}^{m}(t) \right\rangle.$$

$$(5)$$

We approximate the hyperpolarizability of H_2O at $\omega_2 = \omega_q = 3698 \text{ cm}^{-1}$ by the "bond hyperpolarizability" of the free OH bond with cylindrical symmetry. This assumption simplifies eqn (5) by converting it to a form that can be evaluated without the knowledge of molecular hyperpolarizability of all individual water molecules in different environments. Under this assumption, $\beta_{q,\lambda\mu\nu}$ has only two nonvanishing components, $\beta_{\perp,\perp,\parallel}$ and $\beta_{\parallel,\parallel,\parallel}$, where \parallel and \perp denote the body-fixed axes along and perpendicular to the free OH bond direction, respectively: $\beta_{\parallel} \equiv \beta_{\parallel,\parallel,\parallel} = \beta_{\mu\nu\nu} = 2.88 \times 10^{-27} \text{ m}^4 \text{ V}^{-1} \text{ s}$ and $\beta_{\perp} \equiv \beta_{\perp,\perp,\parallel} = \beta_{\mu\nu\nu} = \beta_{\nu\nu\nu} = 0.32\beta_{\parallel}$, which were obtained from Raman and IR measurements. Therefore, the sum over (λ,μ,ν) only has three non-vanishing combinations: $(\hat{u},\hat{u},\hat{w})$, $(\hat{v},\hat{v},\hat{w})$, $(\hat{v},\hat{v},\hat{w})$.

The time-dependent direction cosine matrix is $D_{l\xi} = \hat{l} \cdot \hat{\xi}(t)$, with $\hat{l} = (\hat{x}, \hat{y}, \hat{z})$ the fixed lab coordinates and $\hat{\xi}(t) = (\hat{u}, \hat{v}, \hat{w})$ the time-dependent molecular coordinates of the free OH bond. The water surface normal is along the z-axis of the laboratory coordinates, and the free OH bond forms an angle $\theta(t)$ with

the surface normal at time t, where $\theta(t)$ lies in the interval $[0,\pi]$, and an angle $\phi(t)$ in the interval $[0,2\pi]$ with respect to \hat{x} in the \hat{x},\hat{y} plane. Then the expression of the molecular coordinates in the laboratory coordinates is

$$\hat{u} = \cos \phi \cos \theta \hat{x} + \sin \phi \cos \theta \hat{y} - \sin \theta \hat{z}$$

$$\hat{v} = -\sin \phi \cos \theta \hat{x} + \cos \phi \cos \theta \hat{y}$$

$$\hat{w} = \cos \phi \sin \theta \hat{x} + \sin \phi \sin \theta \hat{y} + \cos \theta \hat{z}$$
(6)

To evaluate the error introduced by finite simulation snapshot time interval, three MD simulations with different snapshot time intervals were used for the calculations, as described below.

In the MD simulations, 1264 water molecules were placed in a rectangular box of dimension $30 \times 30 \times 70 \text{ Å}^3$, where the water section is sandwiched between two sections of vapor along the z-direction. Periodic boundary conditions were used in all directions, but in the z-direction, we sandwiched the water slab with two slabs of vacuum. Water molecules were modeled by the DL_POLY 2 program³⁷ as rigid and nonpolarizable, using the TIP3P potential commonly used for molecular mechanics. 38 The Nosé-Hoover thermostat 39,40 was used to perform the constant NVT MD simulations at T = 298 Kand the SHAKE algorithm⁴¹ was used to constrain the degrees of freedom of rigid water molecules. The time step for integrating Newton's equations is always 1 fs, but it is unnecessary to record the results of each step. Instead, we recorded the instantaneous orientation of all free OH bonds in discrete snapshots, evolving the simulation between snapshots without recording the individual steps. In this work, we saved all of the configurations for the snapshot time interval of 1 fs, and every 10 configurations for a time interval of 10 fs, and every 100 configurations for 100 fs. After adequate equilibration of a random initial configuration, simulated with a time step of 1 fs, three individual simulations each with a different snapshot time interval of either 1 fs, 10 fs, or 100 fs were performed. In the three cases, to generate a total of 40 000 configurations, the total simulation time was 40 ps, 400 ps, and 4 ns, respectively. The correlation functions were calculated using a time average,

$$\langle \alpha(0)\mu(t)\rangle = \frac{1}{T-t}\sum_{\delta t=0}^{T-t}\alpha(\delta t)\mu(t+\delta t),$$

where T is the length of the simulation and δt is the offset time

For sampled configurations of the water/vacuum interface, it is essential to select only the free OH bonds on the water surface that respond to the laser beams in real SFG experiments. Only the free OH bonds at the surface will break the inversion symmetry necessary for an SFG signal. Previous simulation studies^{3,15–18} identified surface free OH bonds as those positioned above a certain cutoff in the *z*-direction. However, as can be seen in Fig. 1, the water surface in the model fluctuates appreciably, and an arbitrary cutoff unavoidably includes the OH bonds in the bulk. Although isotropy due to random orientation of the free OH bond in the bulk will provide a natural surface selection effect, the local field corrections relevant to calculating $A_{\rm eff}$'s only apply to the free OH bonds directly on the surface.⁴³ The correct selection procedure would be to select only those free OH bonds that

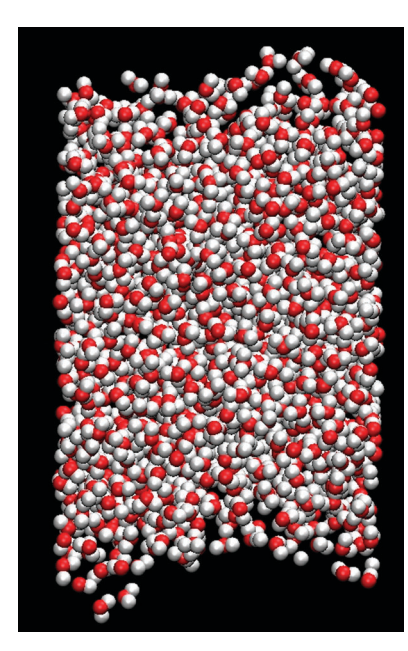


Fig. 1 Snapshot of the simulated water/vacuum interfaces. Black spheres (red, online) represent oxygen atoms, and white ones represent hydrogen atoms.

are both on the surface and those that do not contribute to bulk inversion symmetry. This aspect led us to exclude surface free OH bonds oriented towards the bulk and keep those oriented toward the vapor. Two experimental quantities, the surface density of free OH bonds, $^{44}N_s = 2.8 \times 10^{18} \text{ m}^{-2}$, and their average tilt angle^{9,14,29} of about 35°, guided us in determining free surface OH bonds that affect the SFG results. In this study, the following three criteria were combined to select the free surface OH bonds which lead to agreement with the above two experimental quantities. First, an OH bond is considered on the surface if no oxygen atoms are inside the open cylindrical space above the hydrogen atom with a radius of 1.5 Angstrom (roughly the length of an O-H bond). Second, the OH bond is not H-bonded with any oxygen atoms. An OH bond is considered H-bonded with another oxygen atom if the inter-oxygen distance is less than 3.5 Å (first coordination shell) and simultaneously the O-H···O angle is less than 30° (approximate librational wagging amplitude of the H-bonds). 45 Because of approximations in the dielectric model, some free OH bonds may be inappropriately included. If the bond is oriented with a large angle to the surface normal, in reality it would have a high probability to be effectively canceled out by another OH bond pointing in the opposite direction. Our selection method must produce an orientation ensemble that reflects this potential inversion symmetry. To address this feature, we used a single free parameter in the calculations, a free OH cutoff angle. Bonds with θ_{OH} greater than the cutoff angle were not included in the calculations. In Table 3 the effect of choosing alternative cutoff angles is summarized. A cutoff of 60° simultaneously reproduced best all experimental observables. The free surface OH bonds selected with the above three criteria yield the surface density of free OH bonds and their average angle very close to experimental values, as shown in Table 1 and Table 3, and a similar remark applies to the susceptibilities.

A snapshot of the free surface OH bonds is shown in Fig. 2. Clearly, the free surface OH bonds in the model are sparse and their oxygen atoms do not form a uniform monolayer. The distribution of the cosine function of the tilt angle θ with respect to the surface normal is plotted in Fig. 3. As expected, the three snapshot intervals do not yield a large difference in the cosine distribution, because of the equilibrating prior to the simulation. Because a cutoff of 60° was applied to the tilt angle, $\cos \theta_{OH}$ cannot be smaller than 0.5, as shown in Fig. 3. The plurality of free OH bonds is oriented along the surface normal.

With the surface free OH bonds determined, the experimental observable mode amplitudes were calculated using eqn (1)–(6). Using the damping constant $\Gamma_q/(2\pi c) = 14.5 \text{ cm}^{-1}$ and normalizing by the simulation surface area, 6,29 the data so obtained are compared with the experimental values29 and listed in Table 2. All ratios of the calculated mode amplitudes are nearly within the measured error of the experimental ratios $A_{\text{eff}}(ssp): A_{\text{eff}}(ppp): A_{\text{eff}}(sps) = 1:0.28 \pm 0.04:0.05 \pm 0.02.$

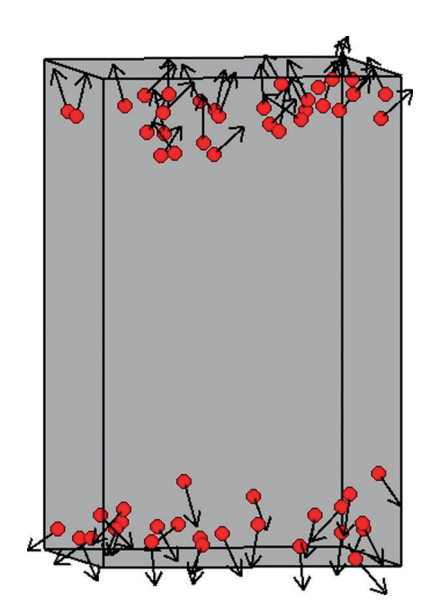


Fig. 2 Snapshot of the chosen free surface OH bonds. Black spheres (red, online) represent oxygen atoms and the vectors point from oxygen atoms to the bound hydrogen atoms. The vectors are elongated for clearer illustration.

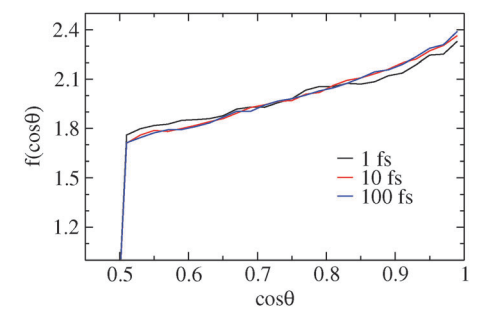


Fig. 3 Probability density of the cosine of the tilt angle with respect to the surface normal, using a cutoff angle of 60°. The three MD simulations with different snapshot intervals of 1, 10, and 100 fs, respectively, result in very similar cosine distributions.

Table 2 Mode amplitudes and their ratios calculated from MD simulations and comparison with the experimental values. A_{eff} has units 10^{-9} m² V⁻¹ s

Mode amplitudes	1 fs	10 fs	100 fs	Experimental
$A_{\text{eff}}(ssp)$	0.17	0.35	3.5	1.7
$A_{\text{eff}}(ppp)$	0.05	0.11	1.0	0.48
$A_{\text{eff}}(sps)$	0.002	0.01	0.3	0.09
$A_{\text{eff}}(ssp)$: $A_{\text{eff}}(ppp)$: $A_{\text{eff}}(sps)$	1:0.30:0.01	1:0.32:0.03	1:0.30:0.08	$1:0.28\pm0.04:0.05\pm0.02$

Table 3 Simulation results depend on free OH cutoff angle, calculating based on the data with the snapshot interval of 1 fs. A cutoff of 60° produces experimental results for a number of free OH, $\langle n_{\rm OH} \rangle$, average orientation angle, $\langle \theta_{\rm OH} \rangle$, and effective susceptibilities. $A_{\rm eff}$ has units 10^{-9} m² V⁻¹ s

Cutoff angle $\langle n \rangle$	$i_{\mathrm{OH}}\rangle$ $\langle heta$	$\theta_{ m OH} angle$	$A_{\text{eff}}(ssp)$: $A_{\text{eff}}(ppp)$: $A_{\text{eff}}(sps)$
45° 16 60° 26 90° 46 Experiment ²⁹ 25	6 38 6 54	8° 4°	0.07:0.035:0.001 (1:0.52:0.02) 0.17: 0.05:0.002 (1:0.30:0.01) 0.40:0.005:0.004 (1:0.01:0.001) $1.7:0.48:0.09 (1:0.28 \pm 0.04:0.05 \pm 0.02)$

The largest amplitudes in Table 3, the $A_{\text{eff}}(ssp)$ and $A_{\text{eff}}(ppp)$, correspond to the incident IR laser being p-polarized. In p-polarization, the electric field vector is parallel to the plane of incidence and therefore probes free OH's that are nearer to the surface normal, and these free OH's are those with the most orientational anisotropy. The $A_{\text{eff}}(ssp)$ is about three times larger than the $A_{\text{eff}}(ppp)$, perhaps reflecting the factor of three difference between β_{\parallel} and β_{\perp} . The $A_{\text{eff}}(sps)$ is smaller than the other two, presumably because with the incident s-polarization, the IR tends to probe free OH's that are closer to being flat on the surface.

Results and discussion

The detailed information of the microscopic structure and dynamics of water/vacuum interface provided by the computer simulations provide some insight into the physical meaning of the three experimental observable mode amplitudes, the average orientation, and free OH bond surface density. Our results, shown in Table 2, achieve good agreement with observed ratios, and they are also within an order of magnitude of experimentally measured results. Because the 1 fs snapshot interval led to a total integration time of 40 ps, which may be too short to adequately generate statistics (others have used multiple nanoseconds⁴²), those results would expectedly differ from the longer simulation times. Although Wei and Shen obtained agreement in the calculated ratios of $A_{\text{eff}}(ssp): A_{\text{eff}}(ppp)$ by assuming the rotational dynamics of θ_{OH} are very fast compared to the vibrational lifetime, they arrived at precisely $A_{\text{eff}}(sps) = 0.29$ Our calculations produce a small but non-zero $A_{\text{eff}}(sps)$, which we plan to investigate more fully comparing the slow approximation limit of the present equations. We will determine this further in future calculations. Although Gan et al. 14 suggest the free OH bonds rarely orient perpendicularly to the surface, their results assumed the distribution of angles to be Gaussian, with a width of about 15 degrees, instead of using a distribution similar to the one calculated in Fig. 3. By calculating the distribution of the bonds and employing a cutoff, we obtain good agreement in the ratio of effective susceptibilities. We also show that not all free OH bonds are necessarily SFG

active, and this may be a source of discrepancy between theoretical measurements of bond orientations and the narrower results from experiments. ¹⁴ As expected, $A_{\text{eff}}(ssp)$ is the largest component because it represents the IR laser coupling directly to the component of the free OH bond oriented perpendicularly to the surface, the orientation with the largest anisotropy. Future work will reveal more information when we extend the overall results and compare them with the slow and fast approximations of the present equations.

Based on the present MD simulations of the air/water interface with the TIP3P empirical water model, the amplitudes and their ratios of the effective nonlinear susceptibilities $(A_{\text{eff}}$'s) were calculated for different polarization combinations and compared with sum-frequency generation (SFG) experiments. Free surface OH bonds are selected as the OH bonds (1) which are not hydrogen-bonded to other oxygen atoms; (2) whose title angles with respect to the surface normal are smaller than 60°; and (3) no oxygen atoms are above the hydrogen atom. With this definition of free surface OH bonds, the calculated average surface density and average tilt angle closely match the experimental values. The calculated absolute values of the experimental observable mode amplitudes differ, while the ratios are relatively similar. The water model presented here was utilized to capture the dynamic orientational distribution of surface free OH bonds. Although the present water model, TIP3P, may be satisfactory for predicting dangling surface OH bonds, there are indications from unpublished work that it predicts too many dangling OHs in bulk water, compared with experiments for non-bonded OH bonds. Measurements of non-bonded OHs in bulk water have been reported by Eaves et al.46 For studies of bulk reaction dynamics, an alternative to the TIP3P model should be explored. We are investigating how the SPC/E model, 47 which has been used for bulk water structure, will alter the calculated susceptibilities. Due to the SPC/E model being better at predicting bulk water properties, we expect the enhanced correlation to bring the susceptibilities even closer to experimental results. We have not considered the effects of capillary fluctuations on the calculated effective susceptibilities, and this will be investigated in a future publication on SFG. In addition, future simulations calculating ensemble averages of correlation functions, instead of effective time averages, may reduce artifacts leading to variations in the calculated susceptibilities between snapshot lengths. This simulation study adds to the theoretical insight into the microscopic structure of the vacuum/water interface, and the present results provide useful information in supporting the recent theory of on-water heterogeneous catalysis.²⁸

Conclusion

In the present paper, in summary, we have formulated the SFG equations in a form where molecular dynamics (MD) calculated quantities can be directly compared with hyperpolarizability (polarizability-dipole) coefficients, A_{eff} , extracted from the experimental data for different types of polarization combinations of the infrared, visible, and reflected light. Preliminary MD results were obtained and the extracted information compared with the experimental data, both in the comparison of ratios of A_{eff} 's and also for comparison with their absolute values. The SFG results were interpreted in terms of physical concepts, for use in exploring other issues and with additional water models. Data from independent sources, infrared and Raman experiments, has been used, in conjunction with SFG theory, to calculate the SFG susceptibility coefficients. In this way, the overall SFG problem was divided into two parts, rather than calculating ab initio the quantum mechanical values of the dipole moment and polarizability derivative. They, in practice, can be computed separately or, as above, evaluated from independent experimental data.

Acknowledgements

It is a pleasure to dedicate this article to the master of surface phenomena, friend and colleague, John Albery, on the occasion of his 75th birthday. The various authors received their support from different sources and they are pleased to acknowledge this support.48

References

- 1 Y. R. Shen and V. Ostroverkhov, Chem. Rev., 2006, 106, 1140.
- 2 P. Jungwirth and D. J. Tobias, Chem. Rev., 2006, 106, 1259.
- 3 C. J. Mundy and I. F. W. Kuo, Chem. Rev., 2006, 106, 1282.
- 4 T. M. Chang and L. X. Dang, Chem. Rev., 2006, 106, 1305.
- 5 G. L. Richmond, Chem. Rev., 2002, 102, 2693.
- 6 Y. A. Mantz, F. M. Geiger, L. T. Molina and B. L. Trout, J. Phys. Chem. A, 2001, 105, 7037.
- S. Narayan, J. Muldoon, M. G. Finn, V. V. Fokin, H. C. Kolb and K. B. Sharpless, Angew. Chem., Int. Ed., 2005, 44, 3275.
- 8 F. Niu, C.-C. Liu, Z.-M. Cui, J. Zhai, L. Jiang and W.-G. Song, Chem. Commun., 2008, 2803.
- Q. Du, R. Superfine, E. Freysz and Y. R. Shen, Phys. Rev. Lett., 1993, 70, 2313.
- 10 F. Vidal and A. Tadjeddine, Rep. Prog. Phys., 2005, 68, 1095.
- 11 C. Y. Lee, J. A. Mccammon and P. J. Rossky, J. Chem. Phys., 1984, 80, 4448.
- 12 K. B. Eisenthal, Chem. Rev., 1996, 96, 1343.

- 13 S. Gopalakrishnan, P. Jungwirth, D. J. Tobias and H. C. Allen, J. Phys. Chem. B, 2005, 109, 8861.
- 14 W. Gan, D. Wu, Z. Zhang, R. Feng and H. Wang, J. Chem. Phys., 2006, **124**, 114705.
- 15 L. X. Dang and T. M. Chang, J. Chem. Phys., 1997, 106, 8149.
- 16 A. Morita and J. T. Hynes, Chem. Phys., 2000, 258, 371.
- 17 V. Buch, J. Phys. Chem. B, 2005, 109, 17771.
- 18 R. S. Taylor, L. X. Dang and B. C. Garrett, J. Phys. Chem., 1996, 100, 11720.
- A. Perry, C. Neipert, B. Space and P. B. Moore, Chem. Rev., 2006, 106, 1234.
- L. F. Scatena, M. G. Brown and G. L. Richmond, Science, 2001,
- 21 M. G. Brown, D. S. Walker, E. A. Raymond and G. L. Richmond, J. Phys. Chem. B, 2003, 107, 237.
- 22 I.-F. W. Kuo, C. J. Mundy, B. L. Eggimann, M. J. McGrath, J. I. Siepmann, B. Chen, J. Vieceli and D. J. Tobias, J. Phys. Chem. B, 2006, 110, 3738.
- 23 H.-S. Lee and M. E. Tuckerman, J. Phys. Chem. A, 2009, 113,
- 24 E. C. Brown, M. Mucha, P. Jungwirth and D. H. Tobias, J. Phys. Chem. B, 2005, 109, 7934.
- A. Perry, C. Neipert, C. Ridley and B. Space, Phys. Rev. E: Stat., Nonlinear, Soft Matter Phys., 2005, 71.
- 26 A. Morita and J. T. Hynes, J. Phys. Chem. B, 2002, 106, 673.
- 27 B. M. Auer and J. L. Skinner, J. Phys. Chem. B, 2009, 113, 4125.
- Y. Jung and R. A. Marcus, J. Am. Chem. Soc., 2007, 129, 5492.
- 29 X. Wei and Y. R. Shen, Phys. Rev. Lett., 2001, 86, 4799.
- 30 D. S. Walker, D. K. Hore and G. L. Richmond, J. Phys. Chem. B, 2006. 110. 20451.
- X. Zhuang, P. B. Miranda, D. Kim and Y. R. Shen, Phys. Rev. B: Condens. Matter, 1999, 59, 12632.
- 32 X. Wei, S. C. Hong, X. W. Zhuang, T. Goto and Y. R. Shen, Phys. Rev. E: Stat. Phys., Plasmas, Fluids, Relat. Interdiscip. Top., 2000,
- 33 Yuki Nagata and S. Mukamel, J. Am. Chem. Soc., 2010, 132, 6436.
- 34 P. N. Butcher and D. Cotter, The Elements of Nonlinear Optics, Cambridge University Press, 1990.
- 35 B. M. Auer and J. L. Skinner, J. Chem. Phys., 2008, 129, 214705.
- 36 Y. R. Shen, The Principles of Nonlinear Optics, J. Wiley, 2000.
- W. Smith and T. R. Forester, The DL_POLY 2 User Manual, CCLRC, Daresbury Laboratory, Daresbury, Warrington, England,
- 38 W. L. Jorgensen, J. Chandrasekhar, J. D. Madura, R. W. Impey and M. L. Klein, J. Chem. Phys., 1983, 79, 926.
- 39 S. Nosé, Mol. Phys., 1984, 52, 255.
- 40 W. G. Hoover, Phys. Rev. A: At., Mol., Opt. Phys., 1985, 31, 1695.
- 41 J. P. Ryckaert, C. G. and H. J. C. Berendsen, J. Comput. Phys., 1977, **23**, 327.
- 42 S. Mukamel, Principles of Nonlinear Optical Spectroscopy, Oxford University Press, 1995.
- 43 P. Ye and Y. R. Shen, Phys. Rev. B, 1983, 28, 4288.
- 44 Q. Du, E. Freysz and Y. R. Shen, Science, 1994, 264, 826.
- 45 A. Luzar and D. Chandler, Phys. Rev. Lett., 1996, 76, 928.
- 46 J. D. Eaves, J. J. Loparo, C. J. Fecko, S. T. Roberts, A. Tokmakoff and P. L. Geissler, Proc. Natl. Acad. Sci. U. S. A., 2005, 102, 13019
- 47 H. J. C. Berendsen, J. R. Grigera and T. P. Straatsma, J. Phys. Chem., 1987, 91, 6269.
- The One Hundred Talents Program of the Chinese Academy of Sciences, the Senior Visiting Scholar Program of the Chinese Academy of Sciences, the General Program of the National Natural Science Foundation of China (No. 10974208), WCU program (R31-2008-000-10055-0) through the National Research Foundation of Korea, the Biological Imaging Center of the Beckman Institute at California Institute of Technology, and also by the National Science Foundation, the Office of Naval Research, and the Army Research Office.